

NUMERICAL SIMULATION OF FREE SURFACE FLOW IN A CHANNEL WITH RIBBED BOTTOM

T. Bodnár and K. Kozel
Department of technical mathematics, Faculty of mechanical engineering,
Czech Technical University in Prague

Introduction

Numerical simulation of free-surface flows is one of the most complicated tasks of CFD. Up to now several methods have been developed for this kind of simulations. Short overview of these methods including the original references could be found e.g. in [4]. There are two main groups of methods applied to the free-surface resolution.

Interface tracking methods define the free-surface as a sharp interface whose motion is followed. The interface forms a part of the computational domain boundary and thus the mesh must be readjusted as the free-surface evolves. *Interface capturing methods* work on fixed grid, which extends beyond the free-surface. The shape of the free-surface is determined by cells which are partially filled.

In general, interface tracking methods are more accurate than interface capturing methods and more efficient for very simple physical situations. However, the interface tracking methods are usually limited only to these very simple situations. With the increasing need to solve very complex cases, the necessity of use of interface capturing methods has arisen.

Therefore the method we have used in our study is based on one of the possible implementations of interface capturing methods. The case solved here is the flow in a 2D channel with ribbed bottom (see Fig. 4), which is partially filled by the water. Because of the action of the inertia and gravity forces, the water-air interface is deformed in proximity of ribs. The shape of the free-surface is relatively simple in this case, however its correct resolution at high Reynolds number in a fully turbulent flow is a very complicated task.

Mathematical Model

The approach used in our model is based on the assumptions for variable-density incompressible flow. It means the flow is treated as if the domain is filled by only one fluid, which density is variable. The discontinuity in density profile arises at the free-surface. The key point in the modeling of this kind of flows is the appropriate formulation of mass conservation law, i.e. in the choice of adequate form of continuity equation. In this case the full "compressible" version should be used.

Mass conservation

$$\frac{\partial \rho}{\partial t} + \operatorname{div}(\rho \mathbf{v}) = 0 \quad (1)$$

Using the chain rule, this could be rewritten as:

$$\frac{\partial \rho}{\partial t} + \mathbf{v} \cdot \text{grad } \rho = -\rho \text{ div } \mathbf{v} \quad (2)$$

Because of the incompressibility assumption, the right-hand side of equation (2) should be equal zero. From this directly follows the expression on the left-hand side is then also equal zero. This means that the mass conservation in variable-density incompressible flows requires two separate conditions to be fulfilled:

a) *Density transport equation*

$$\frac{\partial \rho}{\partial t} + \mathbf{v} \cdot \text{grad } \rho = 0 \quad (3)$$

b) *Divergence-free constrain*

$$\text{div } \mathbf{v} = 0 \quad (4)$$

The equation (3) is used to control the time-evolution of liquid relative mass-fraction. So it could be simply rewritten as

$$\frac{\partial r}{\partial t} + \mathbf{v} \cdot \text{grad } r = 0 \quad (5)$$

Here $r = r_L$ for liquid and $r = r_G$ for gas. Because of the linearity of equation (5) we have some freedom in choice of values r_L and r_G . The interface between gas and liquid can thus be found as an isosurface of $r = r_s$, where $r_s = (r_L + r_G)/2$. Using the computed value of r the local volume fraction of liquid could be established as $c_L = (r - r_G)/(r_L - r_G)$ which is in the range from 0 to 1. Using this value the appropriate local material properties (density and viscosity) could be obtained by simple interpolation between the corresponding values of gas and liquid. E.g. for local density the following relation holds:

$$\rho = c_L \rho_L + (1 - c_L) \rho_G \quad (6)$$

This method can be seen as an elementary implementation of VOF method introduced in [8].

To enforce the divergence-free constrain and calculate pressure, the equation (4) is modified by adding the time-derivative of pressure properly scaled by the artificial speed of sound c :

$$\frac{1}{c^2} \frac{\partial p}{\partial t} + \text{div } \mathbf{v} = 0 \quad (7)$$

This model is suitable for computation of steady flow, while the time-marching technique is used to get stationary solution. In such a case the non-physical additional term in the equation (7) disappears and the true solution of the steady problem is recovered.

Reynolds averaged Navier-Stokes equations

The conservation of Reynolds-averaged momentum components results in the following set of equations:

$$\rho \frac{\partial v_i}{\partial t} + \rho v_j \frac{\partial v_i}{\partial x_j} = -\frac{\partial p}{\partial x_i} + \frac{\partial}{\partial x_j} \left[(\mu + \mu_T) \frac{\partial v_i}{\partial x_j} \right] + \rho g_i \quad i = 1, 2, 3 \quad (8)$$

Here μ and μ_T denote the laminar and turbulent viscosities, while g_i stands for gravity acceleration. The components of velocity vector v_i could be computed directly from these equations. The pressure p and density ρ are updated from equations (7) and (5).

Turbulence Model

We have chosen the SST $k - \omega$ turbulence model see e.g. [12]. The model modification adopted here is exactly the one of [7]. This choice was governed by the complex physical phenomenology of the case to be solved. Especially the following problems should be handled in this situation:

- Highly curved flow patterns (see e.g.[7])
- Two-fluid mixture flow (see e.g. [11])
- Flow with complex separation and recirculation regions (see e.g. [12])
- Possible extension for flow over rough wall (see e.g. [6], [5])

The Shear Stress Transport (SST) $k - \omega$ model blends the $k - \epsilon$ and $k - \omega$ models to get more accurate predictions in complex flows. Hereafter the k denotes the turbulent kinetic energy, ϵ is the dissipation rate of k and ω denotes the specific dissipation rate of k . These quantities are linked to turbulent viscosity by the Kolmogorov-Prandtl relation $\mu_T = \rho k / \omega$ which is further generalized in (19). Both $k - \epsilon$ and $k - \omega$ "elementary" models could be written in the common form:¹

$$\rho \frac{\partial k}{\partial t} + \rho v_j \frac{\partial k}{\partial x_j} = P - \beta^* \rho k \omega + \frac{\partial}{\partial x_j} \left[\left(\mu + \frac{\mu_T}{\sigma_k} \right) \frac{\partial k}{\partial x_j} \right] \quad (9)$$

$$\begin{aligned} \rho \frac{\partial \omega}{\partial t} + \rho v_j \frac{\partial \omega}{\partial x_j} &= \frac{\gamma \rho}{\mu_T} P - F_4 \beta \rho \omega^2 + \frac{\partial}{\partial x_j} \left[\left(\mu + \frac{\mu_T}{\sigma_\omega} \right) \frac{\partial \omega}{\partial x_j} \right] \\ &+ 2\rho \frac{1 - F_1}{\sigma_{\omega 2} \omega} \frac{\partial k}{\partial x_j} \frac{\partial \omega}{\partial x_j} \end{aligned} \quad (10)$$

Model constants are slightly different for each of these models. The blending between $k - \omega$ and $k - \epsilon$ model is provided by switching between their parameters .

$$\begin{pmatrix} \sigma_k \\ \sigma_\omega \\ \beta \end{pmatrix} = F_1 \begin{pmatrix} \sigma_{k1} \\ \sigma_{\omega 1} \\ \beta_1 \end{pmatrix} + (1 - F_1) \begin{pmatrix} \sigma_{k2} \\ \sigma_{\omega 2} \\ \beta_2 \end{pmatrix} \quad (11)$$

Here the blending function F_1 reads:

$$F_1 = \tanh(\Gamma^4) \quad \text{with} \quad \Gamma = \min \left[\max \left(\frac{\sqrt{k}}{\beta^* \omega d}; \frac{500\nu}{\omega d^2} \right); \frac{4\rho \sigma_{\omega 2} k}{CD_{k\omega} d^2} \right] \quad (12)$$

The $CD_{k\omega}$ stands for positive part of cross-diffusion term

$$CD_{k\omega} = \max \left[\frac{2\rho}{\sigma_{\omega 2} \omega} \frac{\partial k}{\partial x_j} \frac{\partial \omega}{\partial x_j}; CD_{k\omega \min} \right] \quad (13)$$

¹Because of the lack of the space the notation used here for turbulence model follows exactly the nomenclature used in [7] and reader is referred to that paper for the complete explanation of all symbols.

The cross-diffusion bound should be prescribed (i.e. $CD_{k\omega \min} = 10^{-10}$).

Model constants for $k - \omega$ model are:

$$\sigma_{k1} = 2.0 \quad \sigma_{\omega1} = 2.0 \quad \beta_1 = 0.075 \quad (14)$$

Model constants for $k - \epsilon$ model:

$$\sigma_{k2} = 1.0 \quad \sigma_{\omega2} = 1.168 \quad \beta_2 = 0.0828 \quad (15)$$

Further parameters: $\kappa = 0.41$ and $\beta^* = 0.09$. Parameter γ is computed from:

$$\gamma = \frac{\beta}{\beta^*} - \frac{\sigma_{\omega} k^2}{\sqrt{\beta^*}} \quad (16)$$

Turbulent kinetic energy production is given by

$$P = \left(2\mu_T S_{ij} - \frac{2}{3} \delta_{ij} \rho k \right) \frac{\partial v_i}{\partial x_j} \quad (17)$$

The symmetric part of the velocity gradient is defined as follows:

$$S_{ij} = \frac{1}{2} \left(\frac{\partial v_i}{\partial x_j} + \frac{\partial v_j}{\partial x_i} \right) \quad \text{with norm} \quad |S_{ij}| = \sqrt{2S_{ij}S_{ij}} \quad (18)$$

The turbulent viscosity is evaluated from

$$\mu_T = \frac{a_1 \rho k}{\max(a_1 \omega; |S_{ij}| F_2 F_3)} \quad \text{where} \quad a_1 = 0.31 \quad (19)$$

The function F_2 is evaluated from:

$$F_2 = \tanh(\Gamma_2^2) \quad \text{with} \quad \Gamma_2 = \max\left(\frac{2\sqrt{k}}{\beta^* \omega d}; \frac{500\nu}{\omega d^2}\right) \quad (20)$$

The function F_3 is given by:

$$F_3 = 1 - \tanh\left[\left(\frac{150\nu}{\omega d^2}\right)^4\right] \quad (21)$$

The streamline curvature effect is taken into account by the function F_4 , given by the following formula:

$$F_4 = \frac{1}{1 + C_{rc} Ri} \quad \text{where} \quad C_{rc} \approx 3.6 \quad (22)$$

The Richardson number Ri is defined by:

$$Ri = \frac{|\Omega_{ij}|}{|S_{ij}|} \left(\frac{|\Omega_{ij}|}{|S_{ij}|} - 1 \right) \quad (23)$$

Here the anti-symmetric part of the velocity gradient is defined as follows:

$$\Omega_{ij} = \frac{1}{2} \left(\frac{\partial v_i}{\partial x_j} - \frac{\partial v_j}{\partial x_i} \right) \quad \text{with norm} \quad |\Omega_{ij}| = \sqrt{2\Omega_{ij}\Omega_{ij}} \quad (24)$$

Boundary conditions

The boundary conditions for the presented model were chosen according to the original paper [7]. The model allows to set boundary conditions on impermeable wall depending on the surface roughness.

Rough wall

$$\omega = \frac{u_\tau^2}{\nu} S_R \quad \text{where the friction velocity} \quad u_\tau = \sqrt{\tau_w/\rho} \quad (25)$$

The nondimensional function S_R is given by

$$S_R = \begin{cases} \left(\frac{50}{\max(k_s^+; k_{s\min}^+)} \right)^2 & \text{for } k_s^+ < 25 \\ \frac{100}{k_s^+} & \text{for } k_s^+ \geq 25 \end{cases} \quad (26)$$

In the above equations the nondimensional sand-grain height is:

$$k_s^+ = \frac{u_\tau k_s}{\nu} \quad (27)$$

Its minimal value could be evaluated from

$$k_{s\min}^+ = 2.4 (y_1^+)^{0.85} \quad \text{where} \quad y_1^+ = \frac{u_\tau \Delta d_1}{\nu} \quad (28)$$

In our case the wall was assumed to be ideally smooth, so the value $k_s^+ = k_{s\min}^+$ was used on the wall.

Free stream

The following free stream values for k , ω , and ν_T could be used

$$\omega_\infty = C \cdot V_\infty / L \quad (29)$$

$$\nu_{T\infty} = 10^{-3} \nu \quad (30)$$

$$k_\infty = \nu_{T\infty} \omega_\infty \quad (31)$$

Here $C \approx 1 \div 10$ and L is the characteristic scale of the flow.

Numerical Solution

Numerical solution of the above presented mathematical model is based on finite-volume cell-centered semi-discretization on structured mesh. The time-integration of the resulting system of ordinary differential equations is carried out using explicit Runge-Kutta multistage scheme. Because of the use of the central-differencing in spatial discretization, suitable stabilization technique is used to avoid non-physical oscillations in the solution.

Space Discretization

The computational mesh is structured, consisting of hexahedral primary control volumes. To evaluate the viscous fluxes also dual finite volumes are needed. These have octahedral shape and are centered around the corresponding primary cell faces. See the following figure 1 for the schematic view of such configuration.

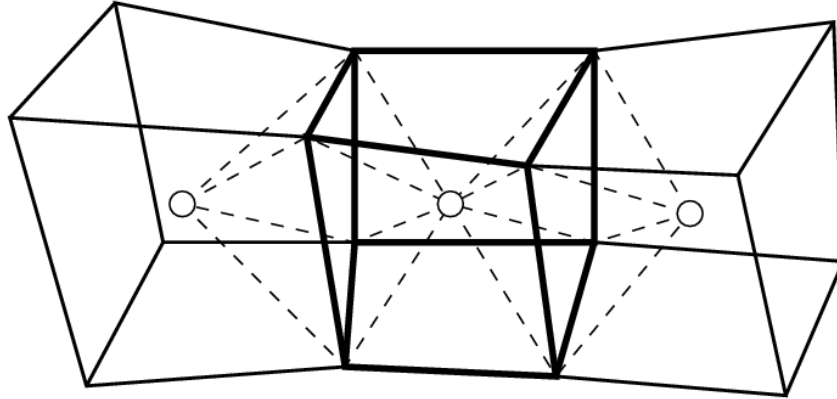


Figure 1: Finite-volume grid in 3D

The system of RANS equations (including the modified continuity equation) could be rewritten in the vector form. Here we use W to denote the vector of unknowns (including pressure). Vectors F , G and H denote the inviscid fluxes in x, y, z directions, while R , S and T stand for their viscous counterparts. Using this notation, the spatial finite-volume semi-discretization could be written in the following form:

$$\frac{\partial W_{ijk}}{\partial t} = -\frac{1}{|D|} \oint_{\partial D} [(F - R), (G - S), (H - T)] \cdot \hat{\nu} dS + \frac{1}{|D|} \int_D f_w \quad (32)$$

Here D denotes the computational cell, $\hat{\nu}$ is the outer unit normal vector of the cell boundary, dS is the surface element of this boundary. The vector f_w contains the external body forces (e.g. gravity in our case). The equation (32) can be rewritten in operator form:

$$\frac{\partial W_{ijk}}{\partial t} = -\mathcal{L} W_{i,j,k} \quad (33)$$

Here \mathcal{L} stands for the finite-volume discretization operator. This operator is still exact at this stage and it should be properly discretized to allow for numerical solution. This is done by the replacement of fluxes in it's formulation by their numerical (approximate) versions.

The inviscid flux integral can be approximated in a central manner, e.g. the value of the flux F on the cell face with index $\ell = 1$ is computed as average of cell-centered values from both sides of this face:

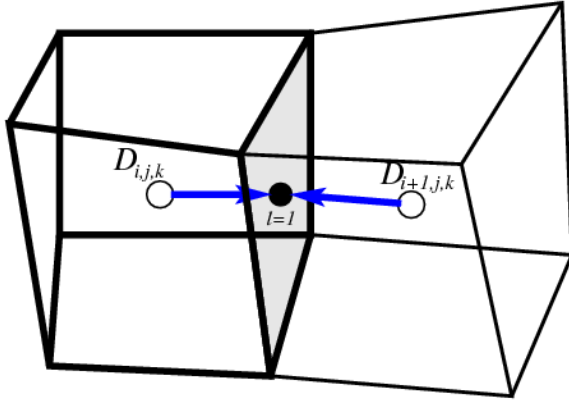


Figure 2: Inviscid flux discretization

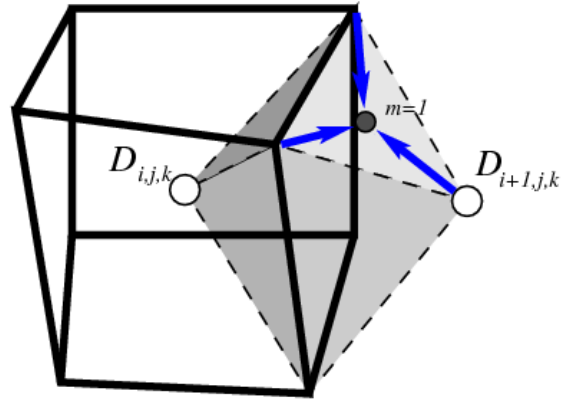


Figure 3: Viscous flux discretization

$$F_1^n = \frac{1}{2} [F(W_{i,j,k}^n) + F(W_{i+1,j,k}^n)] \quad (34)$$

The contribution of inviscid fluxes is finally summed up over the cell faces $\ell = 1, \dots, 6$. In this way we can write down the inviscid flux approximation:

$$\oint_{\partial D} F \nu^x dy dz \approx \sum_{\ell=1}^6 F_\ell \nu_\ell^x S_\ell \quad (35)$$

The discretization of viscous fluxes is a little bit more complicated because the vectors R, S, T were defined using the derivatives of velocity components. So we need to approximate somehow these derivatives at cell faces. This can be done using the dual finite-volume grid that is centered around the corresponding faces (see Figure 1 and 3).

The evaluation of velocity gradient components is then replaced by the surface integral over the dual volume boundary. Finally this surface integral is approximated by a discrete sum over the dual cell faces (with indices $m = 1, \dots, 8$). For example trying to evaluate the first component of the viscous flux R_1 (i.e. approximate u_x) at the cell face $l = 1$ we must proceed in the following way:

$$u_x \approx \oint_{\partial \bar{D}} u \nu^x dy dz \approx \sum_{m=1}^8 u_m \nu_m^x S_m \quad (36)$$

The outer normal of the dual cell faces should be properly approximated $\nu^x \approx \nu_m^x$. The values of velocity components in the middle nodes of these faces are taken as an average of the values in the corresponding vertices.

Time Integration

The problem is now in the semi-discrete form:

$$\frac{dW_{ijk}}{dt} = -\tilde{\mathcal{L}} W_{i,j,k} \quad (37)$$

This system of ordinary differential equations can be solved e.g. by the Runge-Kutta multistage method:

$$\begin{aligned} W_{i,j,k}^{(0)} &= W_{i,j,k}^n \\ W_{i,j,k}^{(r+1)} &= W_{i,j,k}^{(0)} - \alpha_{(r)} \Delta t \tilde{\mathcal{L}} W_{i,j,k}^{(r)} \quad r = 1, \dots, m \\ W_{i,j,k}^{n+1} &= W_{i,j,k}^{(m)} \end{aligned} \quad (38)$$

The three-stage explicit RK scheme has coefficients:

$\alpha_{(1)} = 1/2$, $\alpha_{(2)} = 1/2$, $\alpha_{(3)} = 1$. This scheme is second order only, however it provides extended stability region leading to CFL=2 which improves the overall efficiency of the whole scheme.

The efficiency and robustness of the method could further be increased by modification of the above algorithm. The modification used for simulations presented in this paper follows the Runge-Kutta time integration procedures outlined in [10] and further refined in [9]. The idea behind this modified approach lies in splitting of the space discretization operator into inviscid and viscous part. The inviscid operator is evaluated at each Runge-Kutta stage, while the viscous operator is evaluated just in few stages. This corresponds to the use of different Runge-Kutta coefficients for time integration of inviscid and viscous fluxes. The modified algorithm could thus be written in the following form:

$$\begin{aligned} W_{i,j,k}^{(0)} &= W_{i,j,k}^n \\ W_{i,j,k}^{(r+1)} &= W_{i,j,k}^{(0)} - \alpha_{(r)} \Delta t (\mathcal{Q}^{(r)} + \mathcal{D}^{(r)}) \\ W_{i,j,k}^{n+1} &= W_{i,j,k}^{(m)} \end{aligned} \quad (39)$$

Here the space discretization operator at stage (r) is split as follows:

$$\mathcal{L}W_{i,j,k}^{(r)} = \mathcal{Q}^{(r)} + \mathcal{D}^{(r)} \quad (40)$$

The inviscid flux \mathcal{Q} is evaluated in usual way at each stage

$$\mathcal{Q}^{(r)} = \mathcal{Q}W_{i,j,k}^{(r)} \quad \text{with} \quad \mathcal{Q}^{(0)} = \mathcal{Q}W_{i,j,k}^n \quad (41)$$

The viscous flux \mathcal{D} uses a blended value of from the previous stage and the actual stage according to the following rule:

$$\mathcal{D}^{(r)} = \beta_{(r)} \mathcal{D}W_{i,j,k}^{(r)} + (1 - \beta_{(r)}) \mathcal{D}^{(r-1)} \quad \text{with} \quad \mathcal{D}^{(0)} = \mathcal{D}W_{i,j,k}^n \quad (42)$$

The coefficients $\alpha_{(r)}$ and $\beta_{(r)}$ are chosen to guarantee large enough stability region for the Runge-Kutta method. The following set of coefficients was used for this study:

$$\begin{aligned} \alpha_{(1)} &= 1/3 & \beta_{(1)} &= 1 \\ \alpha_{(2)} &= 4/15 & \beta_{(2)} &= 1/2 \\ \alpha_{(3)} &= 5/9 & \beta_{(3)} &= 0 \\ \alpha_{(4)} &= 1 & \beta_{(4)} &= 0 \end{aligned}$$

It is easy to see that for this four-stage method only two evaluations of dissipative terms are needed which saves significant amount of calculations while retaining the advantage of large stability region of the method. Further admissible sets of coefficients together with comment on the increase of the efficiency and robustness could be found in the original papers [10] and [9] and the references therein.

Numerical Stabilization

It is a well known property of central schemes, that in the presence of strong gradients they produce non-physical oscillations in the solution. There are many ways to avoid this phenomena. The method used here is based on pressure stabilization. This approach is long time used in finite-element community and has been used in finite-volume framework in *Vierendeels, Riemslagh, & Dick* [14]. The main principle of this method is to add a pressure dissipation term (Laplacian) into the modified continuity equation. This helps to prevent oscillations in pressure, which stabilizes the whole numerical method.

The pressure stabilization is introduced by the additional source term on the right-hand side of modified continuity equation. This term has the following form:

$$Q_{i,j,k} = \frac{1}{|D_{i,j,k}|} \sum_{\ell=1}^{2N} \frac{p_{\ell} - p_{i,j,k}}{b_{\ell}} S_{\ell} \quad (43)$$

Here ℓ denotes the control volume cell face index, p_{ℓ} is the pressure in the corresponding neighboring cell and S_{ℓ} is the cell face area. The value b_{ℓ} has the dimension of velocity and represents the maximal convective velocity in the domain and local diffusive velocity.

$$b_{\ell} = \max(\sqrt{v_1^2 + v_2^2 + v_3^2}) + \frac{2\nu}{L_{\ell}} \quad (44)$$

Symbol L_{ℓ} corresponds to a distance between the actual and neighboring cell centers.

On an uniform cartesian mesh with cells of size δx this term gives:

$$Q = \frac{\delta x}{2b} \Delta p \quad (45)$$

This type of numerical stabilization has some advantages over the classical artificial diffusion applied to the velocity components. First, its "artificial" effects are clearly separated from the physical viscosity included in RANS equations. Even more important property of this stabilization term is that it contains only second derivatives of pressure and thus it will vanish if pressure will be a linear function of space coordinates. This is the case of e.g. Poiseuille flow with linear pressure decay along the flow axis.

Numerical simulations

Numerical tests were performed for segment of a 2D channel with two ribs of square cross-section. Channel is partially filled by water, while the remaining volume is occupied by air. The geometrical configuration can be seen in the Figure 4. The fully developed velocity profile with maximum speed 0.25, 0.5, 1.0 and 2.0 *m/s* was assumed for both fluids on the inlet. The length scale \mathbf{h} was set to 1*cm*.

In order to avoid complicated multiblock mesh structure, a cartesian grid was used and velocity was set to zero "inside" of the obstacle. This approach simplifies significantly the computation in the case of multiple obstacles. The mesh structure detail can be seen in the

Figure 5.

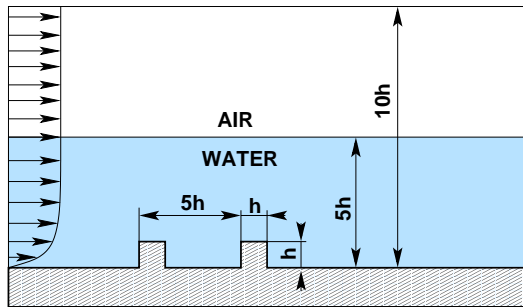


Figure 4: Computational geometry

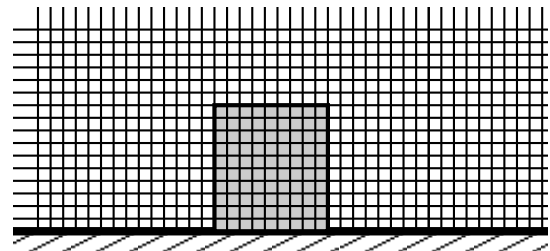


Figure 5: Cartesian grid structure

Conclusions, remarks

The numerical results presented here were chosen to show the resolution of the flow in the proximity of the ribs and the ability of the model to capture the free surface for selected range of inlet velocities.

The numerical results shown in figure 6 show the position of the water surface for the case of the four selected inlet velocities. It is possible to see that the water-air interface shape changes dramatically within the selected range of velocities. On the other hand the shape and size of recirculation zones in the proximity of the square ribs is almost identical for all of the four cases.

More apparent is the difference in the distribution of turbulent kinetic energy shown in the figure 7, where the contours of TKE are drawn for the four studied cases using the same color scale.

From the presented tests of the whole numerical model directly follows that the method used here is applicable for this class of problems. More numerical tests in turbulent flow regime should be performed. Multiple roughness element configurations will be extensively studied in detail. A comparison of presented numerical results of free surface flow with experimental data published e.g. in Chára [3] is under preparation.

Acknowledgment

The financial support for the present project was partly provided by the *Czech Grant Agency* under the *Grant No.103/06/0461* and by the *Research Plan MSM 6840770010* of the *Ministry of Education of Czech Republic*.

References

- [1] BENEŠ, L. & KOZEL, K.: Numerical Simulation of 3D Atmospheric Boundary Layer Flow with Pollution Dispersion. In: *Proceedings of International Conference on Advanced Engineering Design*, (pp. 141–146). University of Glasgow, Glasgow (2001). ISBN 0-85261-731-3.

- [2] BODNÁR, T. & PŘÍHODA, J.: Numerical simulation of turbulent free-surface flow in curved channel. *Journal of Flow, Turbulence and Combustion*, vol. 76, no. 4: (2006) pp. 429–442.
- [3] CHÁRA, Z.: UVP a LDA měření rychlostních polí v okolí překážek umístěných na dně kanálu. In: *XIV. Medzinár. vedecká konferenci Aplikácia experimentálných a numerických metód v mechanike tekutín, Rájecké Teplice*, (pp. 145–150) (2004).
- [4] FERZIGER, J. H. & PERIĆ, M.: *Computational Methods for Fluid Dynamics*. Springer Verlag (1997).
- [5] HELLSTEN, A.: On the solid wall condition of ω in the $k - \omega$ type turbulence model. Tech. rep., Helsinki University of Technology, Dept. of Mech. Eng., Laboratory of Aerodynamics (1998).
- [6] HELLSTEN, A. & LAINE, S.: Extension of $k - \omega$ shear-stress transport turbulence model for rough-wall flows. *AIAA journal*, vol. 36, no. 9: (1998) pp. 1728–1729.
- [7] HELSTEN, A.: Some improvements in Menter's $k - \omega$ SST turbulence model. Tech. rep., American Institute of Aeronautics and Astronautics (1998). AIAA-98-2554.
- [8] HIRT, C. W. & NICHOLLS, B.: Volume of fluid (VOF) method for dynamics of free boundaries. *Journal of Computational Physics*, vol. 39: (1981) pp. 201–221.
- [9] JAMESON, A.: Time Dependent Calculations Using Multigrid, with Applications to Unsteady Flows Past Airfoils and Wings. In: *AIAA 10th Computational Fluid Dynamics Conference, Honolulu* (1991). AIAA Paper 91-1596.
- [10] JAMESON, A., SCHMIDT, W., & TURKEL, E.: Numerical Solutions of the Euler Equations by Finite Volume Methods Using Runge-Kutta Time-Stepping Schemes. In: *AIAA 14th Fluid and Plasma Dynamic Conference, Palo Alto* (1981). AIAA paper 81-1259.
- [11] KAURINKOSKI, P. & HELLSTEN, A.: FINFLO: the Parallel Multi-Block Flow Solver. Tech. rep., Helsinki University of Technology, Dept. of Mech. Eng., Laboratory of Aerodynamics (1998).
- [12] MENTER, F. R.: Two-Equation Eddy-Viscosity Turbulence Models for Engineering Applications. *AIAA Journal*, vol. 32, no. 8.
- [13] RANSAU, S. R.: Solution Methods for Incompressible Viscous Free Surface Flows: A Literature Review. Preprint 3/2002, Norwegian University of Science and Technology, Department of Mathematical Sciences, Norwegian University of Science and Technology, N-7491 Trondheim, Norway (2002).
- [14] VIERENDEELS, J., RIEMSLAGH, K., & DICK, E.: A Multigrid Semi-implicit Line-Method for Viscous Incompressible and Low-Mach-Number Flows on High Aspect Ratio Grids. *Journal of Computational Physics*, vol. 154: (1999) pp. 310–344.
- [15] VIOLLET, P. L.: *Mécanique des fluides à masse volumique variable*. Presses de l'école nationale des ponts et chaussées (1997).

Numerical results

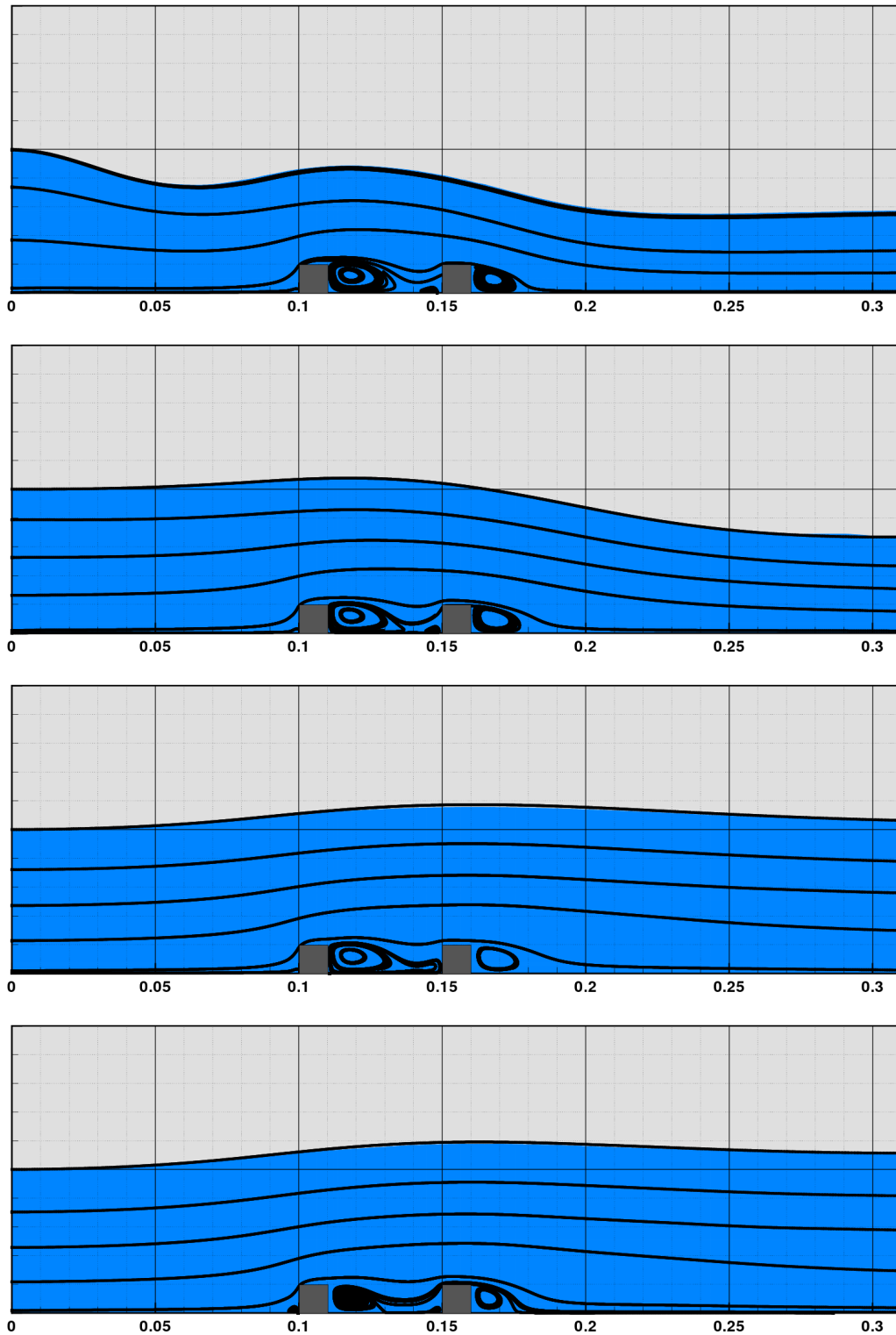


Figure 6: Water level and streamlines for inlet velocities 0.25, 0.5, 1.0 and 2.0 m/s.

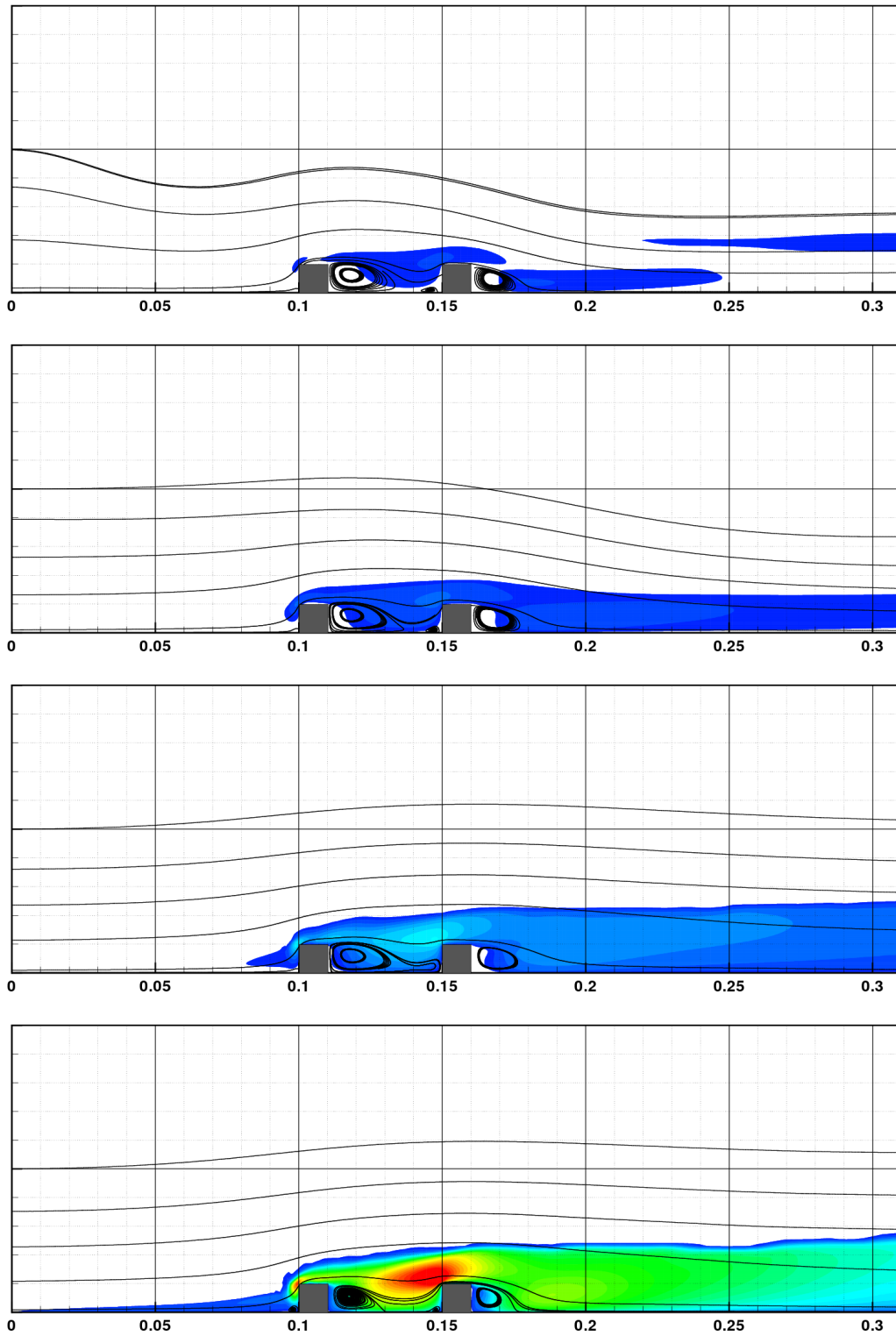


Figure 7: Turbulent kinetic energy and streamlines for inlet velocities 0.25, 0.5, 1.0 and 2.0 m/s.